An auxin-driven polarized transport model for phyllotaxis

Henrik Jönsson*†, Marcus G. Heisler†‡, Bruce E. Shapiro§, Elliot M. Meyerowitz‡¶, and Eric Mjolsness¶‖

*Computational Biology and Biological Physics Group, Department of Theoretical Physics, Lund University, S-221 00 Lund, Sweden; ‡Division of Biology and §Biological Network Modeling Center, California Institute of Technology, Pasadena, CA 91125; and ‖Institute of Genomics and Bioinformatics and Department of Computer Science, University of California, Irvine, CA 92697

Contributed by Elliot M. Meyerowitz, November 12, 2005

Recent studies show that plant organ positioning may be mediated by localized concentrations of the plant hormone auxin. Auxin patterning in the shoot apical meristem is in turn brought about by the subcellular polar distribution of the putative auxin efflux mediator, PIN1. However, the question of what signals determine PIN1 polarization and how this gives rise to regular patterns of auxin concentration remains unknown. Here we address these questions by using mathematical modeling combined with confocal imaging. We propose a model that is based on the assumption that auxin influences the polarization of its own efflux within the meristem epidermis. We show that such a model is sufficient to create regular spatial patterns of auxin concentration on systems with static and dynamic cellular connectivities, the latter governed by a mechanical model. We also optimize parameter values for the PIN1 dynamics by using a detailed auxin transport model, for which parameter values are taken from experimental estimates, together with a template consisting of cell and wall compartments as well as PIN1 concentrations quantitatively extracted from confocal data. The model shows how polarized transport can drive the formation of regular patterns.

Arabidopsis thaliana | computable plant | dynamical model | pattern formation | meristem

In the growing plant shoot, new leaf and flower primordia emerge at well defined positions, resulting in strikingly regular patterns (1). These phyllotactic patterns can be whorled (more than one new primordium develops simultaneously) or spiral (single primordia are created sequentially). Spiral phyllotaxis is often connected to the Fibonacci series because the numbers of parastichies (visible spirals) in each direction around the axis are commonly consecutive Fibonacci numbers. Also, consecutive primordia in the spiral often appear at a divergence angle close to the golden angle. The beautiful symmetries apparent in phyllotaxis and its connection to mathematics have inspired scientists to create theories and models to explain these patterns. One important finding from mathematical analysis and physical simulation (2, 3) is that many of the seemingly complex phyllotactic patterns and transitions found in plants can probably be explained to a large degree by any regular spacing mechanism superimposed on a gradually enlarging generative region. This finding is important because it suggests that the problem can be reduced to two potentially independent and smaller questions. The first question regards how meristem size is determined during plant development. The second question involves how a regularly spaced pattern of primordial position is specified. Traditionally, models have concentrated on the second question, and they can be divided into molecular and mechanical ideas (4–6). Because we investigate a model based on molecular experiments, here we discuss some molecular-based ideas in more detail. Schoute (7) first proposed the idea of lateral inhibition based on a diffusible chemical produced by each developing primordium that inhibits the initiation of primordia nearby. The inhibition hypothesis has been studied extensively in iterative models (3, 8) and has been shown to be capable of producing common phyllotactic patterns for which different parameter values specifying inhibition range relative to a generative region lead to different stable phyllotactic patterns (3). Continuous changes in these parameters were used to investigate transient phases between these patterns relevant to a growing plant (8). Relating back to the work of Turing (9), Meinhardt (10) introduced a reaction–diffusion version of the inhibitor model by incorporating an activator molecule as well as an inhibitor, allowing for a continuous dynamical model. These models exhibit robust and dynamic pattern generation, including the initiation of new concentration peaks corresponding to primordia (10).

An alternative idea is based on competition or depletion of a primordium-promoting factor and was proposed by Preistley and Scott in 1933 (11) and by Mitchison in 1977 (2) and Chapman and Perry in 1987 (12). Recent (and old) findings have provided considerable support for such a depletion scenario. In a series of elegant experiments, it has been shown that the plant hormone auxin (in the form of indole-3-acetic acid) is an essential activator for primordium formation (13, 14). Plants in which auxin transport is blocked (either chemically or in the *pin1* mutant) exhibit a pin-formed morphological phenotype characterized by a lack of primordium development and a bare meristem. This phenotype can be rescued by local application of auxin in the form of a lanolin paste, showing that localized auxin is both necessary and sufficient for primordial development. In the wild type, auxin transport is mediated by the *Arabidopsis* PIN (PINFORMED) family of putative auxin efflux mediators (15) as well as the auxin import mediators AUX1 and its relatives (16). However, the principle protein required for primordium development appears to be PIN1 because *pin1* mutants lack floral primordia in contrast to the relatively mild phenotypes, so far, of other auxin transport mutants. In the shoot apical meristem (SAM), the PIN1 protein is expressed mainly in the epidermal (L1) layer of cells and it is polarized toward newly forming primordia (Fig. 1) (14). In young primordia, PIN1 is polarized downwards into the subepidermal layers, presumably initiating vascular differentiation. In the epidermis below the SAM, PIN1 is polarized upwards toward the SAM, and this polarization depends on the PID (PINOID) protein (17).

Considering these data, Reinhardt *et al.* (14) have proposed that auxin is a primordium activator that is depleted from primordial regions via PIN1-dependent auxin transport so that auxin reaches the next critical threshold for initiation at the point farthest from the previous point of depletion. One limitation of this class of model would appear to be in generating whorled patterns for which multiple positions are specified simultaneously. Another equally important issue not explained by the

Conflict of interest statement: No conflicts declared.

Freely available online through the PNAS open access option.

†H.J. and M.G.H. contributed equally to this work.

¶To whom correspondence may be addressed. E-mail: emj@uci.edu or meyerow@caltech.edu.

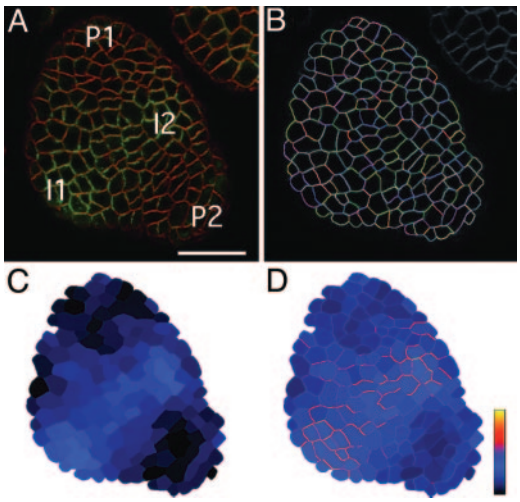

Fig. 1. Template extraction from a confocal image. Shown is a horizontal optical section through the epidermal layer of cells at the shoot apex. (*A*) Original confocal data. The red signal shows a membrane marker, and green shows a PIN1::GFP construct. P1 and P2 marks visible primordia, I1 and I2 show the locations of the next primordia (modified from ref. 20). (Scale bar, 30 μm.) (*B*) Walls extracted by watershed algorithm (cellular compartments inside) visualized on the membrane marker image. (*C*) PIN1 intensities in extracted cell compartments. (*D*) PIN1 intensities in cell/membrane compartments.

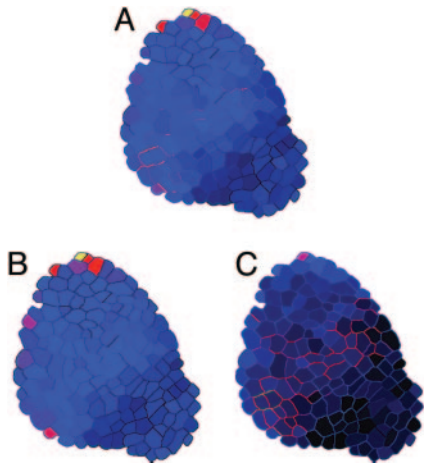

Fig. 2. Auxin equilibrium concentrations for simulations on the template using constant extracted PIN1 concentrations (Fig. 1*D*). (*A*) Wall pH equal to 5, which is the experimentally estimated value. (*B*) Wall pH equal to 4.5. (*C*) Wall pH equal to 5.5.

Reinhardt *et al.* (14) proposal is how auxin transport itself is patterned. The objective of this work is to propose a model for primordial positioning that is based on the assumption that PIN1 polarity is regulated by relative auxin concentrations in neighboring cells within a two-dimensional space, such as the epidermis. The main elements of our model include (*i*) passive and active auxin transport, in which PIN1 mediates auxin efflux; (*ii*) a model for PIN1 cycling between internal and membrane compartments, in which auxin regulates the polarization of PIN1 by modulating the cycling parameters in different directions; and (*iii*) changes in cell adjacency relationships determined by cellular growth and mechanics. The basis for the regulatory model is a feedback mechanism by which cells with relatively high auxin concentrations increase their auxin content by influencing PIN1 polarity in neighboring cells, which as a result become auxin-depleted. Thus, from a close to homogeneous state, auxin peaks emerge at regular distances and determine the locations of early primordia. These mechanisms were simulated on a meristem-like surface topology by using a cell-based model including cellular growth and an elastic mechanics model (18). This model realizes one direction of the two-way interaction between regulatory and mechanical networks outlined in ref. 19. The resulting auxin model generates spiral and whorled phyllotactic-like patterns as found in plants. A more detailed look at the PIN1 polarization dynamics around the formation of a new peak (primordium) shows that the model is capable of predicting the polarization reversal in cells in between the new and older primordia, which has recently been shown in experiments (20).

We also include a detailed auxin transport description based on the chemiosmotic hypothesis of auxin transport using experimental estimates for auxin transport parameter values (21–23). Using this model, we introduce a schema for evaluating and optimizing PIN1 cycling model parameters that compares the model predictions to quantified confocal microscopy data of functional PIN1 protein fused to GFP.

Results

Auxin Transport Model Combined with Extracted PIN1 Localization. We first set out to test the behavior of the detailed auxin transport model (Eq. **3**) by using the geometry and PIN1 localization extracted from a confocal image (Fig. 1). The expectation is that cells forming new primordia have a relatively high auxin concentration. In the model, most of the parameters are taken from experimental estimates, but the strength of active transport and the explicit PIN1 concentrations are unknown. In ref. 21, PIN1 is not explicitly modeled and an anion permeability constant is inferred. We used this value together with a maximal membrane PIN1 concentration set to 1 μmol per unit of area. In addition, production and degradation of auxin is allowed for. The details of the model and parameter values used are provided in *Supporting Methods* (see also Figs. 7 and 8 and Tables 1, 2, and 5, which are published as supporting information on the PNAS web site). The equilibrium auxin concentrations resulting from these parameter values are shown in Fig. 2*A*. As can be seen, the newest visible primordium (P1) has a clear peak in auxin concentration. There is also a low concentration region between the SAM and the next-older visible primordium (P2), but there is no major peak of auxin concentration at this primordium, most likely because the primordium peak is outside the two-dimensional template. It can also be seen that the two primordial positions that form next have small peaks of auxin concentrations (I1 and I2). Thus, the model seems to behave qualitatively as expected.

To investigate how robust this behavior is to different parameter changes, we simulated the model using a range of parameter values around the estimated values (Fig. 2 *B* and *C*; see also *Supporting Methods* and Figs. 9–11, which are published as supporting information on the PNAS web site). The results show that the model exhibits considerable stability and the qualitative results are similar to Fig. 2*A*. As an example, varying the wall pH results in the auxin concentrations shown in Figs. 2 *B* and C. Lowering the wall pH can be interpreted as an approximation to how a symmetric influx mediator may influence the model. The conclusions drawn from these simulations are that the auxin transport model combined with the extracted PIN1 localizations qualitatively behaves as expected and that this behavior is robust.

Auxin-Driven PIN1 Cycling. Our central hypothesis is that the relative concentrations of auxin in neighboring cells differentially drive the polarization of PIN1 to the corresponding portion of the membrane between each cell and its neighbors. To analyze the dynamics of auxin transport in such a model, we simplify the model to a single parameter description. We use the cell-based model and simplify the auxin transport description (Eq. **2**) by

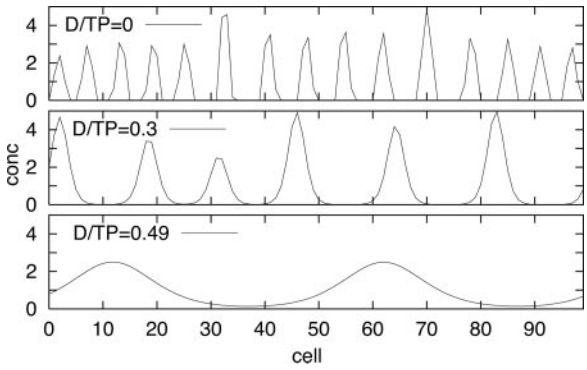

Fig. 3. Simulations of the simplistic model, for which the initial auxin concentrations are [0.999:1.001] and periodic boundary conditions are used. The plots show equilibrium auxin concentrations for simulations with different values of D/TP.

assuming that the PIN1-mediated transport is unsaturated, which leads to a model described by

$$\frac{dA_i}{dt} = D \sum_{k \in \mathcal{N}_i} (A_k - A_i) + T \sum_{k \in \mathcal{N}_i} (A_k P_{ki} - A_i P_{ik}). \qquad [1]$$

$A_i(A_k)$ is the auxin concentration in compartment $i(k)$, whereas P_{ik} and P_{ki} are the PIN1 concentrations on the membrane toward the neighboring compartment. D is the strength of passive transport, and T is the strength of the PIN1-dependent active transport. The summation is over the set of neighbors, $\mathcal{N}_i$, and the only parameters present are the strengths of the passive and active transports. We assume that the total amount of PIN1 in the cell and its membrane is constant and equal for all cells ($P = P_i^{\text{tot}} = P_i + \Sigma_k P_{ik}, \forall i$). We use a linear polarization feedback [$f(A_j) = k_1 A_j$] in Eq. **4** and assume that the PIN1 is in its equilibrium polarization state at any given time, which leads to $P_{ij} = PA_j/[(k_2/k_1) + \Sigma_k A_k]$. Finally, we assume that most PIN1 is situated at the membrane ($k_2 \ll k_1$), which leads to $P_{ij} = PA_j/(\Sigma_k A_k)$ and a model in Eq. **1** only depending on auxin concentrations and the three parameters D, T, and P, which can be treated as a single parameter D/TP.

Fig. 3 shows one-dimensional simulations of the model using periodic boundaries and varying D while keeping TP fixed. The simulations are started with an auxin distribution close to the homogeneous fixed point ($A_i = A, \forall i$), and it can be seen that the model is capable of creating patterns. An increased passive transport rate leads to larger distances between the peaks, and, for large enough D/TP, no pattern is created by the model. To further investigate the behavior of this simplified model, we analyzed the linear stability of Eq. **1** at the homogeneous fixed point (details in *Supporting Methods*; see also Fig. 12, which is published as supporting information on the PNAS web site). The main conclusions from the analysis are that the fixed point is unstable when $D/TP < 0.5$ and that the initial auxin dynamics away from the unstable fixed point has a parameter-dependent spatial wavelength. This simple model illustrates that the feedback in which auxin regulates its own polarized transport leads to nontrivial dynamics from which parameter-dependent regular patterns can form.

Optimizing the PIN1-Cycling Model. As described in *Supporting Methods* (see also Fig. 13, which is published as supporting information on the PNAS web site), the optimization is performed by simulating the detailed auxin model with extracted values of PIN1 concentration; it then uses the equilibrium auxin values for optimizing the PIN1 cycling model parameters [in Eq. **4** using a Hill description for $f(A_j)$] to fit the extracted values. The objective function landscape is quite smooth, resulting in a "simple" optimization problem for which a local search algorithm with multiple restarts is sufficient to find good solutions. In Fig. 4*A* the resulting PIN1 concentrations for the optimized model are plotted directly on the template to be compared with Fig. 1*D*. Fig. 4*B* shows a quantitative comparison between extracted and optimized PIN1 concentrations, with a mean squared error of 0.015. It should be stressed that we use extracted values for the total amount of PIN1 in each cell and that these values are different for individual cells. This variation introduces a bias in the optimization measure. An indication of this bias is given by having each cell uniformly distribute its PIN1 content, which leads to a mean squared error of 0.031. To better appreciate the information in these numbers, more data should be used together with comparisons between different kinds of PIN1 polarization models. In addition, optimization of some of the more uncertain parameters within the auxin transport model can be included in such an approach.

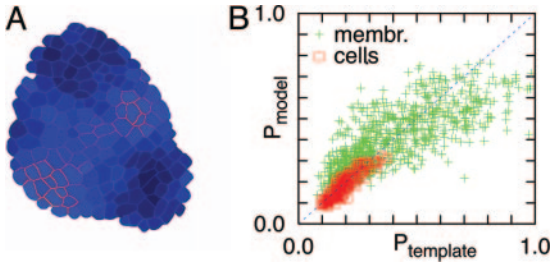

Fig. 4. Example of an optimized PIN1 cycling model. The optimized parameter values are $K = 0.4$, $n = 3.0$, and $k_2/k_1 = 0.4$. (*A*) PIN1 concentration resulting from the optimized model plotted on the template (compare with Fig. 1*D*). (*B*) Quantitative comparison of PIN1 between the template and the model, where the resulting optimized model values are plotted vs. the extracted values for individual compartments.

Phyllotaxis Model on a Simplified Shoot Topology with Growth. To investigate the patterning dynamics of our model on a growing shoot, we simulate the cell-based auxin model in a system where cells are confined to a half-sphere connected to a cylinder. The cellular growth is uniform, the definition of the central zone is dynamic, and the auxin peaks are not fixed. Hence, these simulations should be viewed as an initial test simply to see whether patterning can be maintained in such a situation. Model details and parameter values used are given in the *Supporting Methods*. Time points from simulations for two different parameter sets are shown in Fig. 5. Illustrations of the complete simulations are provided as Movies 1 and 2, which are published as supporting information on the PNAS web site. Fig. 5*A* shows a simulation leading to a spiral-like phyllotaxis, with new peaks forming one at a time, and Fig. 5*B* shows a pattern in which the peaks form in pairs in a whorled-like (decussate) pattern. The parameter difference between the simulations is the size of the defined central zone. It should be noted that the continuation of these patterns is not extremely stable. Typically the temporal order in which new primordia form in the spiral-like pattern can sometimes reverse, and the radial position of the appearance of peaks and the time between the formation of two consecutive peaks are not constant, which can lead to switching between different quasistable patterns in a single simulation. To a large extent, this instability is due to the noise introduced by the growth/mechanical model, which allows for discrete jumps at cell division and local rearrangements of cells (leading to appearance and disappearance of neighbor pairs and the sliding of cells in respect to each other), that is not present in a growing plant. In addition, to achieve more stability, a more appropriate

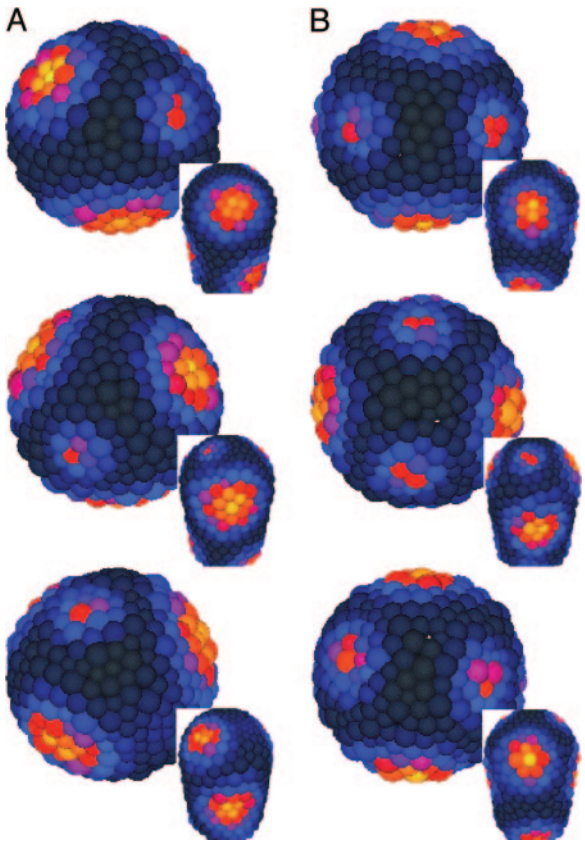

Fig. 5. Simulation of the phyllotaxis model on a half-sphere cylinder surface including cellular growth and proliferation. The main images show a top view (with the insets showing a side view), and time is increasing from top to bottom. The two simulations have different values for the size of the defined central zone. (*A*) Peaks formed in a spiral pattern. (*B*) Peaks formed in a whorled (decussate) pattern.

definition of the central or peripheral zone would probably be required along with fixation of the auxin concentrations (or their effects) in cells once they move out of the peripheral zone. Despite these caveats, the dynamics of the simulations and the resulting patterns show that the model has the potential for generating phyllotactic patterns on a growing tissue such as the plant apical meristem.

PIN1 Polarization Reversal. A characteristic feature of PIN1 behavior during *Arabidopsis* primordium development is that, in cells adaxial to a developing primordium, PIN1 polarity undergoes a reversal from being directed toward the primordium to being directed away from it and toward younger primordia as they are specified in adjacent cells (20). To test whether our model can recapitulate these polarity reversals we examined the dynamics of PIN1 polarization in our cell-based model when a new peak forms by using a two-dimensional system of growing and proliferating cells. Fig. 6 shows cells from such a simulation that are located near to where a new peak forms. It can be seen that polarization reverses in cells located between the older peaks and the newly formed peak, confirming that our model can recapitulate reversals in PIN1 polarity similar to those that are observed in the living plant.

Discussion

We have presented a model for phyllotactic patterning based on a feedback loop between relative auxin concentrations in adjacent cells and auxin efflux direction. When simulating the

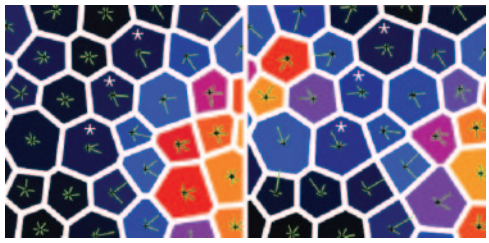

Fig. 6. Simulation of the phyllotaxis model on a two-dimensional plane. Shown is the PIN1 polarization in cells as a new peak is formed. PIN1 polarization (P_{ij}) is shown as bars, with lengths corresponding to a measure of its value, and the color coding shows the auxin concentration. Cells reversing polarity are marked with an asterisk.

cell-based version of the model on a growing shoot-like topology, this model is capable of producing both spiral and whorled patterns and recapitulates observed polarization reversals in the neighborhood of newly formed auxin peaks. These results show that regulation of polarized auxin transport by auxin, together with the mechanics of cell growth and neighborhood change, may provide the underlying mechanisms for phyllotactic patterning. We also present a methodology that bridges the gap between theoretical models and experiments. Unlike previous models for generating phyllotaxis, this model is based on detailed experimental data. Auxin is now established as an essential molecule required for primordium initiation. In turn, its distribution in the shoot apical meristem depends on the activity of the PIN1 putative auxin efflux mediator. Our model includes the chemiosmotic hypothesis of auxin transport, where transport depends on the differential permeability of the protonated and neutral forms of the acid as well as the pH difference between cytoplasm and wall regions (24, 25). This study provides a simulation of our present conception of auxin transport mechanisms on a cellular template derived directly from real tissue. Although PIN1 has not been shown to directly transport auxin, its activity is essential for this process. Thus, we feel that we are justified in using its relative concentrations as a proxy for auxin efflux mediator concentrations. The main limitation of the present technique is that it is limited to two dimensions because of the lack of resolution in the confocal *z* axis. For the purposes of this study, our data are adequate because our model is two-dimensional and is proposed to occur in the meristem epidermis. Although a model limited to two dimensions is inadequate for describing all of the processes that occur in a three-dimensional structure, such as the meristem, data suggest that the L1 layer of the meristem may play a special role in auxin transport and that phyllotactic patterning may occur as an essentially two-dimensional process. First, PIN1 expression is much higher in the epidermis than in underlying cells. Second, PIN1 polarity in these cells is predominantly lateral with basal localization occurring only after localized expression has been established (20, 26). The expression of the auxin influx mediator AUX1 is also limited predominantly to the L1, and removal of the L1 layer essentially abolishes primordial development (14). These data suggest that it is possible that auxin patterning of primordial positions occurs in two dimensions; hence, we feel justified in proposing a two-dimensional model. Recently, it has been shown that auxin can influence PIN1 polarization by reducing endocytosis (27). It is interesting to note that a model with a constant PIN1 exocytosis and an endocytosis reduced by auxin in the neighboring cell can lead to a similar pattern-generating behavior as the model presented. The two models do lead to differences in the detailed dynamics, but these discrepancies are unnoticeable in the current investigation. Elsewhere, it has been reported that auxin can regulate the transcription of both efflux and influx carriers (20, 28, 29). Although we have not

yet included this aspect of regulation into our model, such regulation may strengthen the feedback process leading to localized maxima. If the conditions were such that the addition of this type of feedback were necessary for patterning to occur, regulation of transcriptional response may provide a means to demarcate a peripheral zone where organogenesis occurs exclusively. We note that transcriptional responses to auxin are apparently suppressed in the central zone (30), consistent with this proposal.

Another model for auxin-influenced auxin transport is the well known flux-based canalization model for venation patterns (31, 32). In that model, rather than polarity being determined by auxin concentrations in neighboring cells, polarity is established according to the flux of auxin passing through a cell's membranes. It would seem that once established, a flux-based transport pathway might be hard to reverse. Because polarity reversals are a regular phenomenon associated with primordium development, a flux-based model might require an additional component mediating these reversals, such as the activity of the protein kinase PID, which is known to function as a PIN1 polarity switch (17). It also remains to be shown whether such a model is capable of producing regular patterns, such as those required for organ positioning. Mechanical buckling models, on the other hand, are capable of generating phyllotactic patterns and can explain transitions between patterns and the different primordial shapes that occur in plants (4–6). A role for auxin transport in this type of model has recently been proposed in which stress patterns dictate transport patterns, which then alter auxin levels to further feedback on stress patterns (6). Although an interesting idea, primordial initiation appears surprisingly robust after meristem tissues are disrupted by laser treatments that presumably change stress patterns to a large degree (33, 34). The degree to which such treatments also disrupt auxin levels remains to be determined. Live imaging of PIN1–GFP-expressing meristems after mechanical perturbations should enable an assessment of this proposal.

Lastly, we would like to stress that the presented polarized transport model is useful not only as a model for phyllotaxis. It provides a variant of a pattern-forming, reaction-transport model for which feedback through polarized transport is the underlying mechanism that creates regular patterning with a parameter-dependent length scale. This mechanism could be a potential explanation for other biological systems where patterning appears.

A future challenge will be to incorporate more accurate estimates for passive and carrier-mediated membrane permeabilities and to extend the model to include tissue below the L1 layer. We would also like to find conditions under which the model may give all of the phyllotactic patterns and transitions observed in plants, which will involve understanding the role of the central zone more thoroughly, including how its size changes over time. Perhaps the most important task ahead is to experimentally test the underlying assumption, which is that PIN1 polarizes up auxin concentration gradients between cells of the meristem epidermis.

Methods

Data Template Extraction. To compare and optimize the models with data from real meristems, we extracted relative PIN1 concentrations in cellular and membrane/wall compartments by quantifying GFP fluorescence emitted by a functional PIN1::GFP fusion protein expressed under the PIN1 promoter and imaged by confocal microscopy (for details, see *Supporting Methods*, which is published as supporting information on the PNAS web site). Because we are interested in PIN1 localization in the epidermal layer, we used a two-dimensional horizontal section covering the L1 layer at the apex and the newly forming primordia (Fig. 1*A*). Cell and wall compartments were extracted with a watershed-type algorithm (Fig. 1*B*) (35). PIN1 concentrations were then estimated from the average GFP intensities in the individual extracted compartments (Fig. 1 *C* and *D*).

Auxin Transport Model. Models for chemiosmotic auxin transport in plant cells were developed in refs. 21–23, and we incorporated PIN1 dependence on auxin efflux into a similar model including cellular and wall/membrane compartments. We also applied the model on a system of cellular compartments, in which case we used PIN1 polarization from analytically calculated equilibrium values. We will refer to these model descriptions as the "detailed" and the "cell-based" models, respectively. In both cases we appreciated the fact that auxin can cross a cellular membrane passively and actively. The net auxin flux between two compartments (i, j) separated by a membrane is defined by $J^{\text{tot}}_{i\to j} = J_{i\to j} - J_{j\to i}$, where the individual terms include passive and active transport.

In our cell-based simulations, we have transport between cellular compartments i and j, resulting in a net flux of (Table 1, rows 4 and 5, which is published as supporting information on the PNAS web site)

$$J^{\text{tot}}_{i\to j} = D(A_i - A_j) + T\left(P_{ij}\frac{A_i}{K_{\text{A}} + A_i} - P_{ji}\frac{A_j}{K_{\text{A}} + A_j}\right), \quad [2]$$

where A_i (A_j) is the auxin concentration in compartment i (j), whereas P_{ij} and P_{ji} are the PIN1 concentrations on the membrane toward the neighboring compartment. D is the strength of the passive transport, and T is the strength of the PIN1-dependent active transport. We allow the active transport to be saturable, modeled in a Michaelis–Menten formalism, where K_{A} is the Michaelis–Menten constant. The cell-to-cell transport is to be interpreted as the cellular efflux combined with a symmetrical influx.

In the detailed model, simulated directly on the geometry of the experimental template, we use a more elaborate description of compartment-specific transport parameters where the parameter values are experimental estimates. We use a compartmentalization where cellular (cytosol) compartments are surrounded by wall compartments toward each neighbor separated by a membrane. The model is a development of the models originally proposed by Goldsmith *et al.* (21) and Mitchison (22), and it explicitly accounts for the anion and weak acid forms of auxin, and that the PIN1-mediated anion transport depends on the electrochemical gradient across the plasma membrane. The net auxin flux between a cellular compartment, i, and its neighboring wall compartment, ij is given by (Table 2, rows 4, 5, 7, and 8, which is published as supporting information on the PNAS web site)

$$J^{\text{tot}}_{i\to ij} = (D_{\text{efflux}}A_i - D_{\text{influx}}A_{ij}) + P_{ij}\left(T_{\text{efflux}}\frac{A_i}{K_{\text{A}} + A_i} - T_{\text{influx}}\frac{A_{ij}}{K_{\text{A}} + A_{ij}}\right), \quad [3]$$

where P_{ij} is the PIN1 located at the membrane and the transport parameters are compartment-type-dependent. In addition, we have apoplastic auxin transport modeled as diffusion between neighboring wall compartments. The details of the auxin transport models are given in *Supporting Methods* (see also Figs. 7 and 8, which are published as supporting information on the PNAS web site).

PIN1 Cycling Model. PIN1 is known to cycle between the plasma membrane and internal cellular compartments (36). The signals that govern the rates and direction of this cycling are to a large extent unknown. Here we propose that relative auxin concentrations in neighboring cells are communicated back to a cell to differentially drive PIN1 polarization, creating a

feedback mechanism whereby auxin regulates its own transport. This feedback leads to regular spatial patterns in auxin concentrations, where we assume that the peaks correspond to sites of primordium initiation.

Specifically, the hypothesis for PIN1 cycling is that auxin in a neighboring cell (A_j) induces the cycling from the cellular compartment (P_i) into the membrane located toward the neighboring cell (P_{ij}), which together with a constant internalization is described by (Table 2, rows 9 and 10)

$$\begin{aligned}\frac{dP_{ij}}{dt} &= f(A_j)P_i - k_2P_{ij}\\ \frac{dP_i}{dt} &= \sum_{k\in\mathcal{N}_i}(k_2P_{ik} - f(A_k)P_i),\end{aligned} \qquad [4]$$

where $f(A_j)$ encodes the feedback from auxin in the neighboring cell and should be an increasing function of A_j, whereas k_2 is a constant. The summation is over the set of cell neighbors, $\mathcal{N}_i$, for the cellular compartment i. We use a linear description, $f(A_j) = k_1A_j$, as well as a saturable form allowing for a nonlinear feedback and described by a Hill-type equation, $f(A_j) = k_1[A_j^n/(K^n + A_j^n)]$, where k_1 is the maximal rate and K and n are the Hill constant and coefficient, respectively. This saturable form can be derived from the hypothesis of a combination of quickly equilibrating reactions including a cell–cell communication pathway (Tables 3 and 4, which are published as supporting information on the PNAS web site). Higher auxin in a neighboring cell leads to an increased PIN1 localization at the membrane toward that cell, resulting in a higher auxin transport into that cell. We find that the strength of active transport compared with passive transport determines whether the feedback is strong enough for creating spatial patterns in auxin concentration. When a local auxin maximum is formed, the cells in the maximum deplete auxin from the surrounding cells. However, at a parameter-dependent distance from the maximum, cells tend to have less auxin in them than neighbors on either side. These cells start to transport auxin away from the initial maximum into new maxima, with the end result being the formation of peaks and troughs of auxin concentration in a spatially regular pattern.

Until now there has been a gap between molecular models and experiments for explaining phyllotaxis. New confocal imaging techniques allow a quantitative comparison between models and experiments for essential molecules, which allows the optimization of unknown model parameters by fitting the model to experiments. We used these techniques to infer parameters in the PIN1 cycling model, given the detailed auxin transport model that uses experimental estimates of the parameters (details of the optimization procedure are available in *Supporting Methods*).

Cell-Based Model with Growing and Proliferating Cells. To be able to investigate the model in a growing shoot-like system, we study the cell-based auxin model in a system where individual cells grow and proliferate and are constrained to exist on a half-spherical surface connected to a cylindrical surface below. The cells are modeled as spheres with radial growth, and neighbors are defined as cell pairs with spatial overlap. For simplicity, we used a single growth rate for all cells at the apex. The mechanical interactions are modeled with a repulsive spring force between neighboring cells (18). Cells in the apical region divide as they reach a threshold size. The initial division direction is random on the surface, and then the positions are adjusted by the mechanical neighbor interactions. Although this model provides a simplified growth model for the epidermal layer of the SAM, it does include individual proliferating cells, and it has the property that cells are displaced out of the apical region toward the periphery, just as they are for real meristems. The growth and mechanical models are discussed in more detail in *Supporting Methods*. To avoid peaks forming at the very apex, a central zone and peripheral zone are defined by an additional auxin production term outside the central zone. This implementation is used to break the symmetry of patterning rather than as a valid biological mechanism for defining these zones.

We thank Christophe Godin, Przemyslaw Prusinkiewicz, and Jan Traas for discussions and Jan Traas for sharing unpublished results. This research was supported by U.S. National Science Foundation FIBR Award EF-0330786 and U.S. Department of Energy Award FG02–88ER13873. H.J. was supported in part by the Knut and Alice Wallenberg Foundation through Swegene (Lund, Sweden).

1. Steeves, T. A. & Sussex, I. M. (1998) *Patterns in Plant Development* (Cambridge Univ. Press, New York).
2. Mitchison, G. J. (1977) *Science* **196,** 270–275.
3. Douady, S. & Couder, Y. (1992) *Phys. Rev. Lett.* **68,** 2098–2101.
4. Green, P., Steele, C. S. & Rennich, S. C. (1998) in *Symmetry in Plants*, eds. Jean, R.V. & Barabé, D. (World Scientific, Singapore), pp. 359–392.
5. Shipman, P. D. & Newell, A. C. (2004) *Phys. Rev. Lett.* **92**, art. no. 168102.
6. Shipman, P. D. & Newell, A. C. (2005) *J. Theor. Biol.* **236,** 154–197.
7. Schoute, J. C. (1913) *Ré. Trav. Bot. Néerl.* **10,** 153–235.
8. Douady, S. & Couder, Y. (1996) *J. Theor. Biol.* **178,** 295–312.
9. Turing, A. M. (1952) *Philos. Trans. R. Soc. London B* **237,** 37–72.
10. Meinhardt, H. (1982) *Models of Biological Pattern Formation* (Academic, London).
11. Preistley, J. H. & Scott, L. (1933) *Biol. Rev. Cambridge Philos. Soc.* **8,** 241–268.
12. Chapman, J. M. & Perry, R. (1987) *Ann. Bot. (London)* **60,** 377–389.
13. Reinhardt, D., Mandel, T. & Kuhlemeier, C. (2000) *Plant Cell* **12,** 507–518.
14. Reinhardt, D., Pesce, E. R., Stieger, P., Mandel, T., Baltensperger, K., Bennett, M., Traas, J., Friml, J. & Kuhlemeier, C. (2003) *Nature* **426,** 255–260.
15. Gälweiler, L., Guan, C., Müller, A., Wisman, E., Mendgen, K., Yephremov, A. & Palme, K. (1998) *Science* **282,** 2226–2230.
16. Bennett, M. J., Marchant, A., Green, H. G., May, S. T., Ward, S. P., Millner, P. A., Walker, A. R., Schulz, B. & Feldmann, K. A. (1996) *Science* **273,** 948–950.
17. Friml, J., Yang, X., Michniewicz, M., Weijers, D., Quint, A., Tietz, O., Benjamins, R., Ouwerkerk, P. B., Ljung, K., Sandberg, G., *et al*. (2005) *Science* **306,** 862–865.
18. Shapiro, B. E. & Mjolsness, E. (2001) in *Proceedings of the Second International Conference on Systems Biology* (Omnipress, Madison, WI), pp. 342–351.
19. Mjolsness, E., Sharp, D. H. & Reinitz, J. (1991) *J. Theor. Biol.* **152,** 429–454.
20. Heisler, M., Ohno, C., Das, P., Sieber, P., Long, J. A., Reddy, G. V. & Meyerowitz, E. M. (2005) *Curr. Biol.* **15,** 1899–1911.
21. Goldsmith, M. H., Goldsmith, T. H. & Martin, M. H. (1981) *Proc. Natl. Acad. Sci. USA* **78,** 976–980.
22. Mitchison, G. J. (1980) *Proc. R. Soc. London Ser. B* **209,** 489–511.
23. Kramer, E. M. (2004) *Trends Plant Sci.* **9,** 578–582.
24. Rubery, P. H. & Sheldrake, A. R. (1974) *Planta* **118,** 101–121.
25. Raven, J. A. (1975) *New Phytol.* **74,** 163–172.
26. Benková, E., Michniewicz, M., Sauer, M., Teichmann, T., Seifertová, D., Jürgens, G. & Friml, J. (2003) *Cell* **115,** 591–602.
27. Paciorek, T., Zazimalova, E., Ruthardt, N., Petrasek, J., Stierhof, Y. D., Kleine-Vehn, J., Morris, D. A., Emans, N., Jurgens, G., Geldner, N., *et al.* (2005) *Nature* **435,** 1251–1256.
28. Vieten, A., Vanneste, S., Wiśniewska, J., Benková, E., Benjamins, R., Beeckman, T., Luschnig, C. & Friml, J. (2005) *Development (Cambridge, U.K.)* **132,** 4521–4531.
29. Schrader, J., Baba, K., May, S. T., Palme, K., Bennett, M., Bhalerao, R. P. & Sandberg, G. (2003) *Proc. Natl. Acad. Sci. USA* **100,** 10096–10101.
30. de Reuille, P. B., Bohn-Courseau, I., Ljung, K., Morin, H., Carraro, N., Godin, C. & Traas, J. (2006) *Proc. Natl. Acad. Sci. USA* **103,** 1627–1632.
31. Sachs, T. (1981) *Adv. Bot. Res.* **9,** 151–162.
32. Mitchison, G. J. (1980) *Proc. R. Soc. London Ser. B* **207,** 79–109.
33. Reinhardt, D., Frenz, M., Mandel, T. & Kuhlemeier, C. (2003) *Development (Cambridge, U.K.)* **130,** 4073–4083.
34. Reinhardt, D., Frenz, M., Mandel, T. & Kuhlemeier, C. (2005) *Development (Cambridge, U.K.)* **132,** 15–26.
35. Jönsson, H., Heisler, M., Reddy, V. G., Agraval, V., Gor, V., Shapiro, B. E., Mjolsness, E. & Meyerowitz, E. M. (2005) *Bioinfomatics* **21,** i232–i240.
36. Geldner, N., Friml, J., Stierhof, Y. D., Jürgens, G. & Palme, K. (2001) *Nature* **413,** 425–428.